DISCLAIMER

This report was prepared as an account of work sponsored by an agency of the United States Government. Neither the United States Government nor any agency thereof, nor any of their employees, makes any warranty, express or implied, or assumes any legal liability or responsibility for the accuracy, completeness, or usefulness of any information, apparatus, product, or process disclosed, or represents that its use would not infringe privately owned rights. Reference herein to any specific commercial product, process, or service by trade name, trademark, manufacturer, or otherwise does not necessarily constitute or imply its endorsement, recommendation, or favoring by the United States Government or any agency thereof. The views and opinions of authors expressed herein do not necessarily state or reflect those of the United States Government or any agency thereof. Reference herein to any social initiative (including but not limited to Diversity, Equity, and Inclusion (DEI); Community Benefits Plans (CBP); Justice 40; etc.) is made by the Author independent of any current requirement by the United States Government and does not constitute or imply endorsement, recommendation, or support by the United States Government or any agency thereof.

INL/RPT-23-70965

Simulation Study of Monoenergetic Photon Source LiDAR System Performance for Emergency Response Applications

January 2023

Scott J. Thompson
David L. Chichester
James T. Johnson

Idaho National Laboratory

INL is a U.S. Department of Energy National Laboratory operated by Battelle Energy Alliance, LLC

INL/RPT-23-70965

Simulation Study of Monoenergetic Photon Source LiDAR System Performance for Emergency Response Applications

Scott J. Thompson
David L. Chichester
James T. Johnson

January 2023

Idaho National Laboratory
Nuclear Nonproliferation Division
Idaho Falls, Idaho 83415

http://www.inl.gov

Prepared for the
U.S. Department of Energy
National Nuclear Security Administration
Office of Defense Nuclear Nonproliferation R&D
Under DOE Idaho Operations Office
Contract DE-AC07-05ID14517

Page intentionally left blank

SUMMARY

The following report summarizes the results of a Monte Carlo simulation and modeling study of the Lawrence Berkeley National Laboratory's (LBL) Monoenergetic Photon Source (MPS) as part of a high-energy LiDAR system for use in emergency response applications. A set of image quality indicators (IQI) and nonsensitive phantoms or generalized surrogates for search targets have been identified for use in the planned measurement campaign at the Berkeley Lab Laser Accelerator (BELLA) Center toward the end FY2023. These items were modeled and the time-of-flight (TOF) spectral responses following irradiation were calculated for a set of varying operating conditions. The goal of this study was to both predict the LiDAR system performance as well as determine if minor modifications to the IQI and phantom designs were required before fabrication. It was found that the IQI and target designs both overlap and extend towards the limit of performance of the system and are thus suitable for the final project measurement campaign.

Page intentionally left blank

CONTENTS

FIGURES

TABLES

Page intentionally left blank

Simulation Study of Monoenergetic Photon Source LiDAR System Performance for Emergency Response Applications

1. INTRODUCTION

The following report documents the simulation and modeling campaign performed at Idaho National Laboratory to assess the testing suitability of identified objects representative of typical Nuclear Nonproliferation Emergency Response (ER) imaging targets. These objects have been chosen for use in the Monoenergetic Photon Source Light Detection and Ranging (MPS Lidar) project's end-of-current lifecycle measurement campaign to be performed in the later part of FY2023 at Lawrence Berkeley National Laboratory's BELLA Center. The objects can be categorized into two sets. The first is a set of image quality indicators (IQI's) designed to assess system performance. The second set are a collection of nonsensitive phantoms or surrogates of sensitive items that require emergency response interdiction and imaging. Specifications regarding the object geometries are described in Section 2. MCNP6 models of these objects were generated and simulations of the resultant photon backscatter signal from the MPS source were calculated. Modeling and simulation details are provided in Section 3.

2. IMAGE QUALITY INDICATORS AND PHANTOMS

2.1 Duplex Plates

Traditionally image spatial resolution is determined in standard radiographs using a set of duplex wires of increasing width and spacing. The smallest observable pair is reported as the resolution and reported for the vertical and horizontal directions in units of line pairs per mm. The MPS contributions to spatial resolution in the horizontal and vertical directions will be dominated by collimation and other standard beam conditioning treatments. This project is therefore primarily concerned with determining the potential axial resolution along the depth profile of a target using the MPS.

A target was designed analogous to a duplex wire to determine an observable form of resolution in the axial or 'z' direction. The design is comprised of interchangeable plates and blank spacers of varying thicknesses that in effect make a set of duplex plates to be positioned normal to the beam direction. A 3D rendering of the target design is provided in Figure 1. The simulated plates in this study were modeled as tungsten, however plates of multiple materials will be fabricated in preparation for the final measurement campaign to determine the system's ability to distinguish between varying electron densities in a potential target.

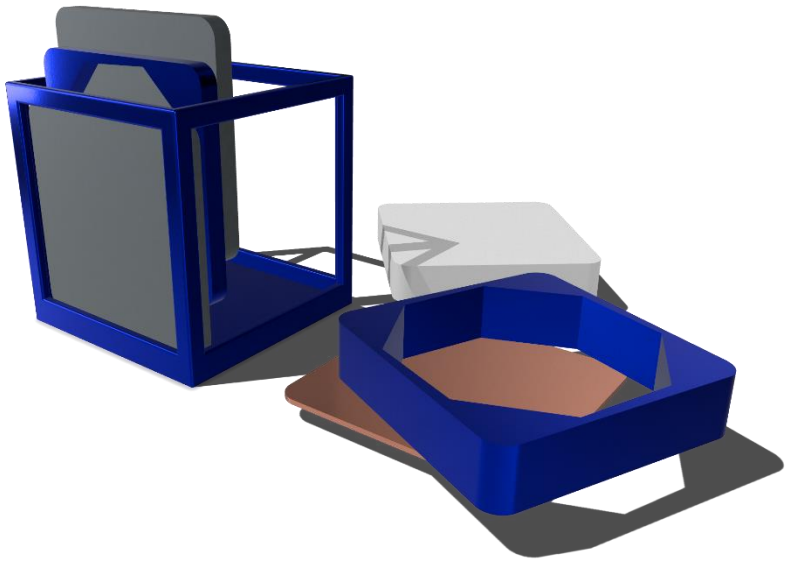

Figure 1. A solid model rendering of the duplex plate target design including various materials and spacers.

2.2 Concentric Spheres

A set of inspection items are required to serve as simplified and unclassified surrogates for emergency response application search targets of sensitive design to test the lidar system in the open access BELLA Center. The INL team maintains a Bonner Sphere style neutron spectrometer manufactured by ELSE Nuclear and shown in **Error! Reference source not found.**. Three of the 7-inch diameter spheres were chosen as potential targets because of their multilayered design. The parameters of these spheres are provided in Table 1.

Figure 2. INL's multi-sphere neutron spectrometer system.

Table 1. Design parameters for the concentric sphere inspection objects.

Sphere ID	Center Sphere	Middle Layer	Outer Layer
7A	4-inch diam. HDPE	0.5-inch Pb	1.0-inch HDPE
7B	4-inch diam. HDPE	0.5-inch Cu	1.0-inch HDPE
7C	3-inch diam. HDPE	1.0-inch Pb	1.0-inch HDPE

(7a) (7b) (7c)

Figure 3. Photographs of the three concentric sphere inspection objects.

3. MODELING AND SIMULATIONS

3.1 Simulation Parameters

Measurement geometries were modeled with the inspection object as the only scattering target to isolate and understand the lidar signal. Each target was freestanding in air at 100 cm from the detector plane. This distance was measured from the center of the spherical objects and from the front face of the duplex plate targets. Backscattered flux was calculated in two concentric rings centered on the beam axis. The smaller angle backscattered flux was tallied on a cylindrical surface with inner diameter of 15 cm and an outer diameter of 25 cm, while larger angle backscatters were tallied on a similar surface with inner diameter of 25cm and outer diameter of 35 cm. A sample cross section of the geometry is shown in **Error! Reference source not found.**. The MPS source energy was modeled with a gaussian distribution with mean energy 2.8 MeV and spread of 0.2 MeV. The left side of **Error! Reference source not found.** shows an overlay of a recently linear scan of the beam dose under the currently configured collimation scheme. The MPS physical source distribution was modeled using the shown gaussian fit to this data with an approximate full-width at half-maximum (FWHM) of 8 cm. Operation of the system with this wide of a beam spot would be potentially useful for large area scans, however it was quickly determined that further collimation would

be required to resolve targets with significant curvature, and therefore a second round of simulations was performed with a narrower FWHM of 0.5 cm. A discussion of this is later provided in Section 3.2. The MPS pulse width is less than 40 fs wide, insignificant when compared to the timing resolution of the detection system, and therefore all photons were emitted simultaneously in the models. Each geometry was initially run for 1E11 particles to minimize Monte Carlo error, requiring 2.5E5 CPU-hours to calculate. Results were scaled by a factor of 1E7 source photons to represent per-pulse values.

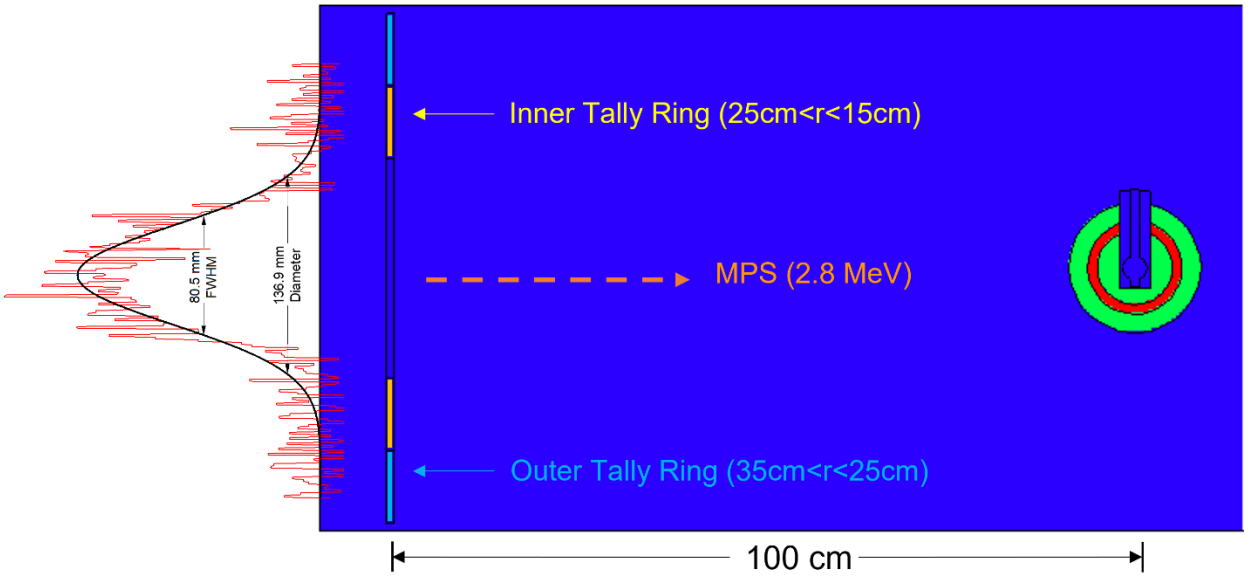

Figure 4. Cross section of the simulation geometry with an overlay of the modeled beam spread.

3.2 Analysis

Previous efforts in the MPS Lidar project have demonstrated the significance of positronium (Ps) lifetime has on the lidar signal. Unfortunately, MCNP6 does not account this physics and a correction to the calculations was required. This was accomplished by isolating flux contributions stemming from annihilation events. The isolated annihilation spectra were then convolved with standard decay spectra: 10% of the intensity was convolved with a half-life of 0.12 ns to account for the para-positronium state and 30% of the intensity was convolved with a half-life of 2.0 ns to account for the ortho-positronium state. The remaining 60% intensity was left unchanged to account for direct annihilation events that do not involve the creation of positronium. The three annihilation spectra were then added back to the calculated backscatter signal. **Error! Reference source not found.** provides a comparison of the backscatter signal with and without the positronium corrections. The positronium decay causes not only a decrease in peak feature backscatter intensities, but also generates significant post-interaction tailing that has the potential to mask backscatter features at later times.

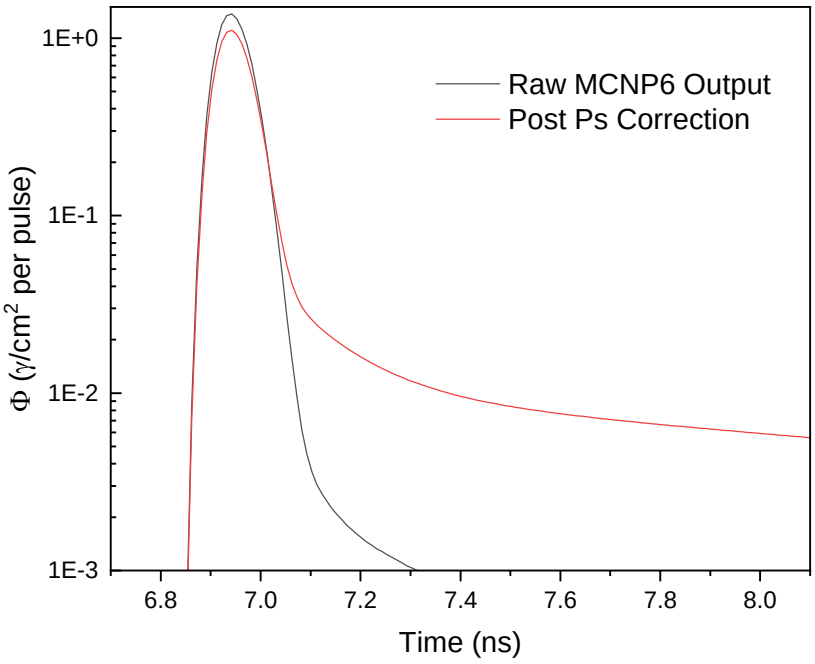

Figure 5. Before and after spectra comparison for the positronium lifetime correction.

At the time of this simulation study, it was still unclear what level of timing resolution would be achievable from the MPS Lidar detection system. To better study the possible performance of the system in a real-world scenario, the simulated backscatter spectra were also convolved with a set of resolutions that span what is believed to be the final resolution range. The spectra were convolved with gaussian distributions with full-width half-maximum values of 25, 50, 75, and 100 ps. **Error! Reference source not found.** demonstrates the effects of timing resolution on the calculated backscatter spectrum. There are two clear scattering targets in the raw MCNP6 spectrum (colored in grey). As the resolution increases the separation between the target peaks fills and creates a feature resulting in a single feature that would require curvature analysis to extract geometric information.

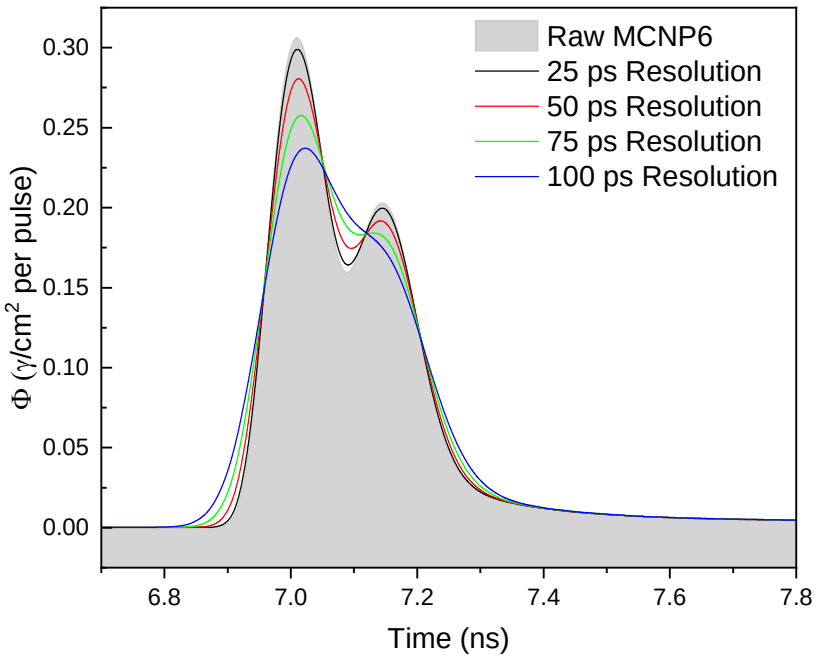

Figure 6. An example comparison of timing resolution effects on a backscatter spectrum.

The duplex plate data set was analyzed using a figure-of-merit calculation used with standard duplex wire IQIs that determines the level of separation between identical wires and is referred to as "dip." Dip is calculated using the following equation:

$$D\% = 100 * (A + B - 2C)/(A + B).$$

For the duplex plate backscatter spectra, the parameters A, B, and C represent the first plate peak intensity, the second plate peak intensity, and the value of least intensity in the time period between the spectral features respectively. These parameters are indicated on a sample spectrum in **Error! Reference source not found.**.

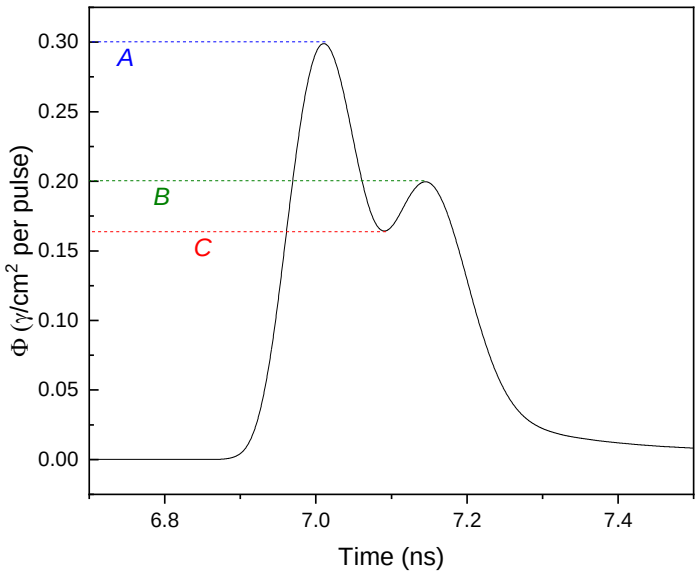

Figure 7. The three parameters used to calculate Dip value.

Upon initial assessment of the duplex plate data, it became apparent that the system would be unable to resolve the thick plates with even the best detector resolutions. The simulated tests were reconfigured using only 1mm thick tungsten plates with increasing spacing. While this test does not provide a direct correlation to standard spatial resolution tests, it does provide insight into the system's ability to discriminate between downstream scattering targets.

The primary goal of the spherical object tests was to identify the various layers of each target. Standard spectroscopic methods for finding peaks or other spectral features that are obscured or hidden by nearby features typically start with taking a simple second derivative as an initial step. The second derivative identifies changes in curvature at local minima and maxima that may correspond to a buried peak or it's tails. **Error! Reference source not found.** has two examples of backscatter spectra and their corresponding second derivatives. As with the duplex plate configurations, upon initial analysis of the emergency response application targets it became apparent that changes were required to the simulation parameters. The curvature of the spheres necessitated a much narrower beam spot to reveal the layered structure of the sphere in the measured lidar signal. The beam width was reduced to a 0.5 cm FWHM before repeating the calculations. **Error! Reference source not found.** shows the change in calculated backscatter spectra for the 7C target with the narrower collimation. Changes in curvature are more easily identified in the measured signal resulting several features in the second derivative that cannot be seen with the original collimation. The blue region at approximately 6.6 ns in this figure highlights examples of the enhancement using the narrower source. While this narrow beam was required to reveal detailed aspects of the target's geometry, it should be noted that the wider beam signal is still capable of identifying gross details that would allow for a large area scan mode of operation prior to a high-resolution narrow-beam scan.

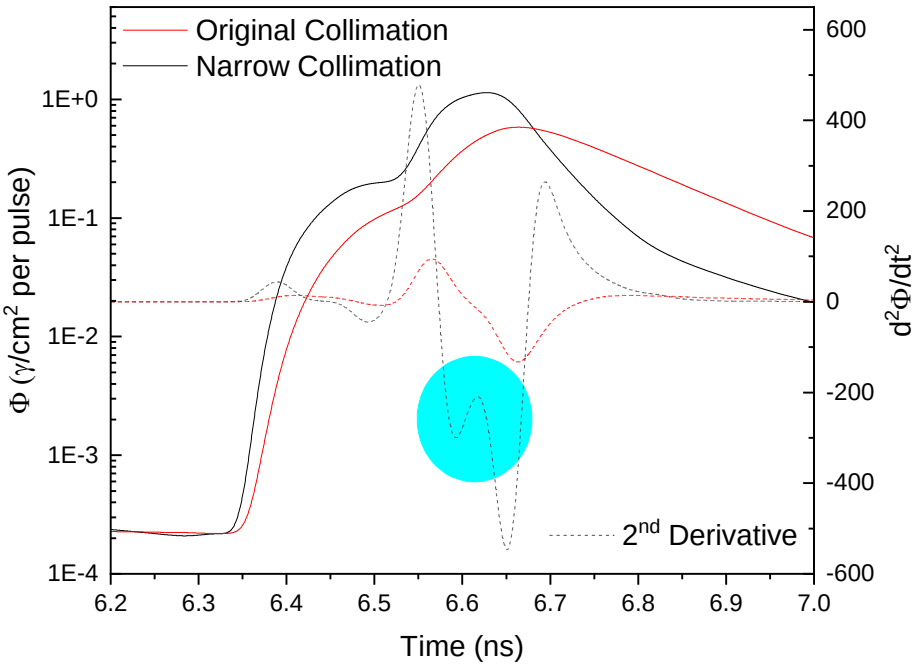

Figure 8. Comparison of the backscatter spectra from the 8-cm FWHM and 0.5-cm FWHM collimation schemes. Dashed lines are the second derivative with respect to detection time. The light blue region highlights features present with the narrow beam but not the original.

4. Results and Conclusions

A notable finding from both the duplex plate and the emergency response application configurations is that the narrow angle detection surface provided a higher level of spectral detail than the larger angle surface. **Error! Reference source not found.** shows the deference between the two tally surfaces for the 2-cm spaced duplex plates. The narrow-angle detections occur approximately 100 ps prior to the wide-angle detections stemming from the same scattering target due to the difference in flight path distance. The dip between plates is also much more pronounced for the narrow-angle detector surface. These results demonstrate the need to both locate the detection system as close to the beam axis as possible as well as the need to position correct each detector pixel when converting from time-of-flight to target depth.

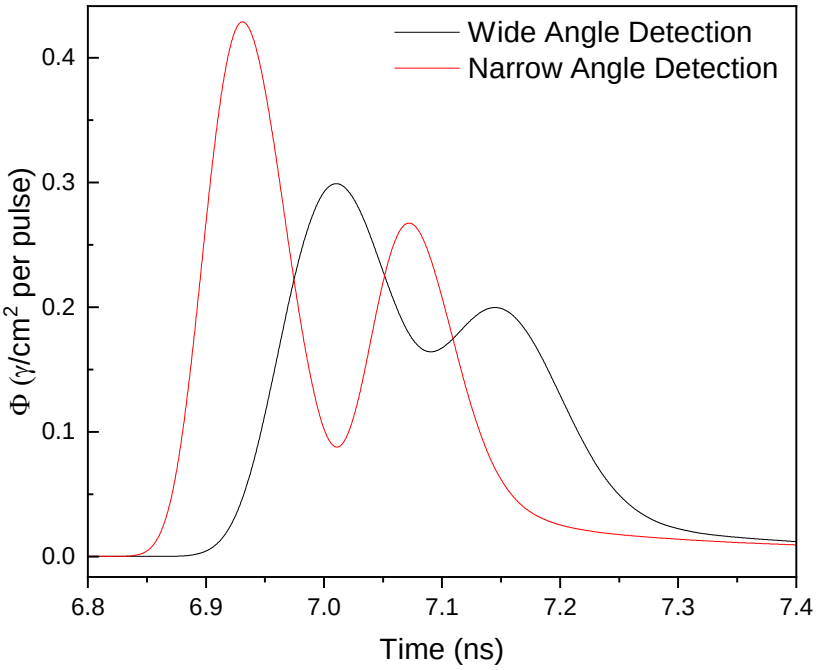

Figure 9. Comparison of calculated backscatter spectra between the inner (narrow angle) and outer (wide angle) cylindrical tally surfaces.

4.1 Duplex Plate Configurations

Simulations were performed for plate spacings of 0.1, 0.2, 0.5, 1.0, and 2.0 cm. The 2.0-cm configuration produced the only spectra for which the two scattering peaks were resolvable and a dip value could be calculated. **Error! Reference source not found.** summarizes the results of the dip value calculations. Traditional duplex wire-based methods for determining the spatial resolution of a digital radiograph involve finding the largest wire pair for which the dip value drops below 20%. While the measurement configurations are not a direct correlation to these methods, we can use this threshold as an indicator to determine the spacing at which the plates can be clearly resolved. At all calculated detector resolutions using the narrow-angle detection surface the dip is above this threshold, indicating that the plates can be resolved somewhere between 1 and 2 cm apart. Using the wider-angle detection surface the 20% threshold is broken between 50 and 75 ps timing resolution, portending that the plates can be also resolved for spacing below 2 cm if the timing resolution of the system is below 50 ps, but increased distance between the plates is required to resolve them at higher resolutions. It should be noted that the analyses described here are preliminary. Along side the development of technology for this project is the development of signature analysis methodologies using deconvolution techniques. The performance characteristics calculated here only represent the system's limitations using basic and traditional analysis methods.

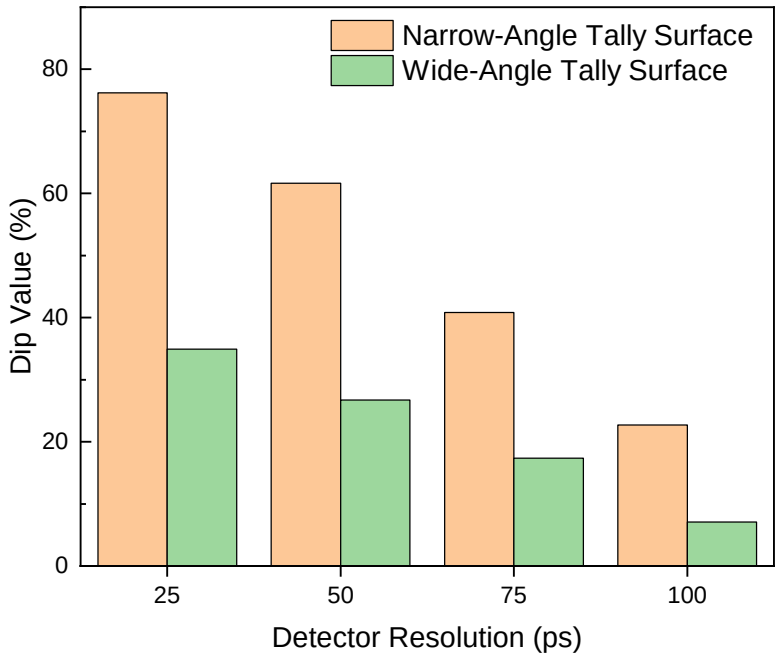

Figure 10. Dip value calculations as a function of detector timing resolution for the 20 mm spaced duplex plates.

The duplex plane target will be modified from its original design for the end-of-project measurement campaign. Tungsten thicknesses of greater than 1 or 2 mm will prove unnecessary. In addition to tests described here, tests will be performed where the spacing will be filled with materials of lower electron density to determine how lower differentials in density affect the dip value and distance required to resolve the two plates. Steel and aluminum plates will be fabricated at greater thickness to test the system's ability to resolve duplex plates of equivalent thickness and spacing, as originally modeled with tungsten, to better correlate to a traditional spatial resolution value.

4.2 ER Application Configurations

Analysis of the three spherical targets described in Table 1 was performed using the narrow-angle detection spectra. Figure 11. Backscatter signalFigure 11, Figure 12, and Figure 13 hold the calculated backscatter signal from targets 7A, 7B, and 7C respectively. The second derivative with respect to time is also provided in each of these plots to help identify changes in curvature representing layer thresholds. The detectable layers have been highlighted in blue (high-density polyethylene), red (lead), and orange (copper). Above each of these plots is positioned a top-half cross section through the center of each target. These cross sections have been loosely sized and positioned to help define what the highlighted layers represent. In all three figures the back side of the outer poly shell is irresolvable using simple preliminary analysis techniques. The deepest resolvable layers of target 7C (that with the thickest center layer of lead, Figure 13) produce little to no indication of curvature in the second derivative of the backscatter signal. When comparing objects 7A and 7B with identical layer thicknesses but different center layers (lead in 7A and copper in 7B) it can be noted that the interface between polyethylene and lead produces a much stronger peaking action in the backscatter signal than polyethylene and copper interface.

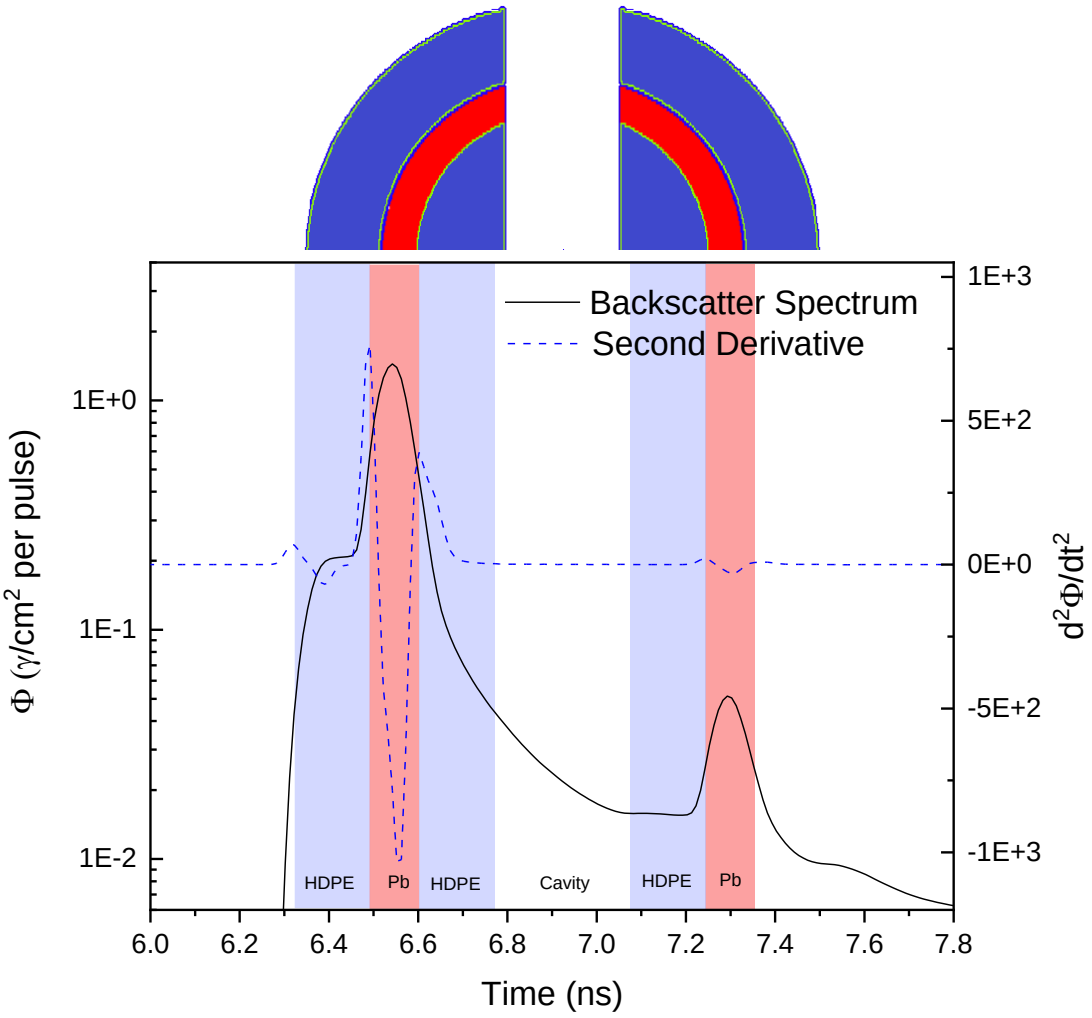

Figure 11. Backscatter signal and its second derivative for test object 7A. Identified layers have been highlighted and labeled and a cross section geometry is provided above the figure to demonstrate how the corresponding layer interfaces are configured in the target geometry.

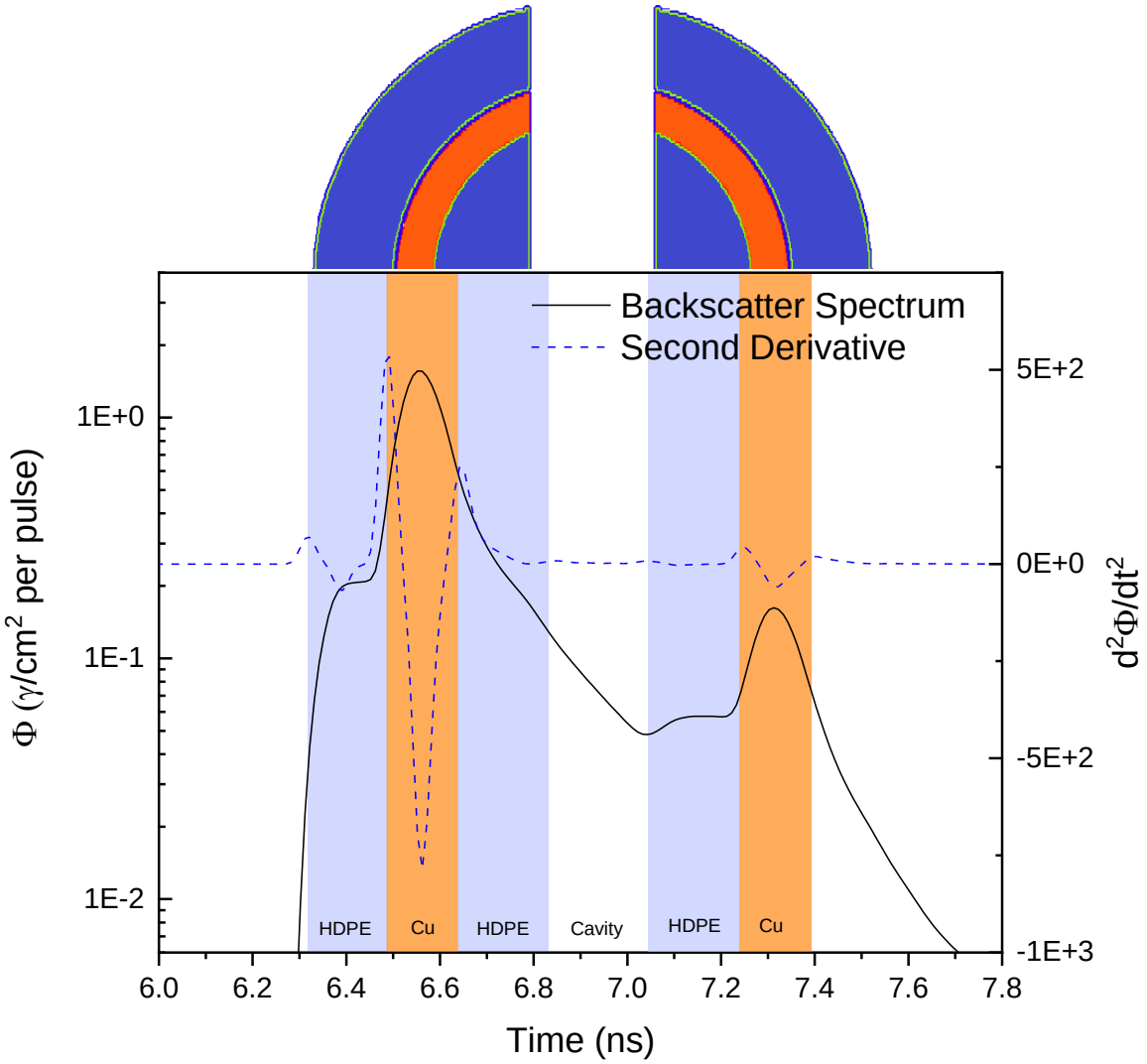

Figure 12. Backscatter signal and its second derivative for test object 7B. Identified layers have been highlighted and labeled and a cross section geometry is provided above the figure to demonstrate how the corresponding layer interfaces are configured in the target geometry.

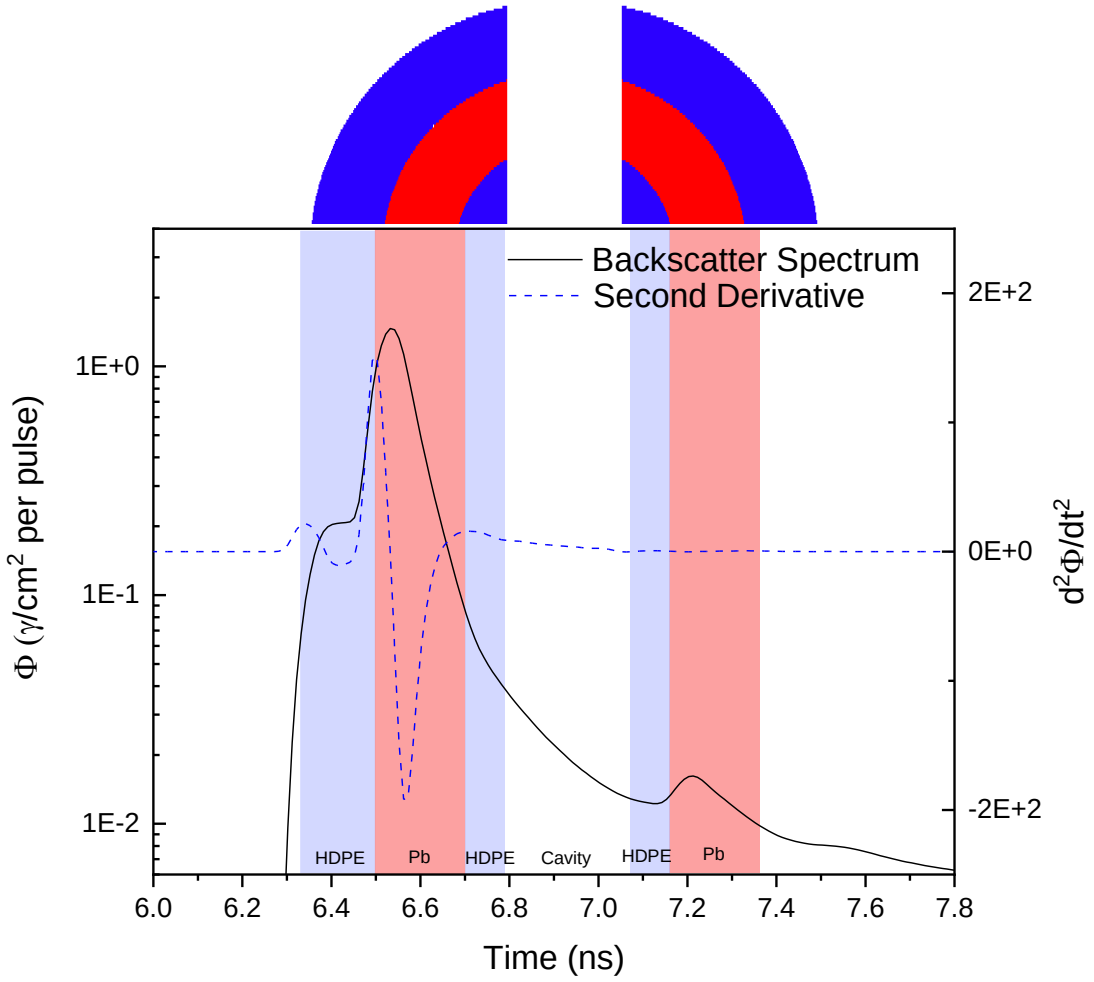

Figure 13. Backscatter signal and its second derivative for test object 7C. Identified layers have been highlighted and labeled and a cross section geometry is provided above the figure to demonstrate how the corresponding layer interfaces are configured in the target geometry.

The simulation and modeling results demonstrate how the identified targets will be ideal for the planned end-of-project measurement campaign. Both the duplex plate target set and the spherical ER surrogate objects cover and extend beyond the performance space of the MPS Lidar system. This will both allow for the project team to adjust system parameters to improve performance during the campaign and allow for the testing and development of signature analysis methods using the collected data.

This research made use of the resources of the High Performance Computing Center at Idaho National Laboratory, which is supported by the Office of Nuclear Energy of the U.S. Department of Energy and the Nuclear Science User Facilities under Contract No. DE-AC07-05ID14517.